Endothelial glycocalyx hyaluronan biosynthesis and function in microcirculation

Wang, G.

CHAPTER 4

Shear stress regulation of endothelial glycocalyx structure is determined by glucobiosynthesis

Gangqi Wang, Sarantos Kostidis, Gesa L. Tiemeier,Wendy M.P.J. Sol, Margreet R. de Vries, Martin Giera, William C. Aird, Peter Carmeliet, Bernard M. van den Berg and Ton J. Rabelink

Arterioscler Thromb Vasc Biol 2020 Feb;40(2):350-364

Abstract

Objective: Endothelial cells exposed to laminar shear stress express a thick glycocalyx on their surface that plays an important role in reducing vascular permeability and endothelial anti-inflammatory, anti-thrombotic and anti-angiogenic properties. Production and maintenance of this glycocalyx layer is dependent upon cellular carbohydrate synthesis, but its regulation is still unknown.

Approach and Results: Here, we show that biosynthesis of the major structural component of the endothelial glycocalyx, hyaluronan (HA), is regulated by shear. Both *in vitro* as well as in *in vivo,* HA expression on the endothelial surface is increased upon laminar shear and reduced when exposed to oscillatory flow, which is regulated by KLF2. Using a CRISPR-CAS9 edited small tetra cysteine tag to endogenous HAS2, we demonstrate increased translocation of HAS2 to the endothelial cell membrane during laminar shear. HA production by HAS2 was shown to be further driven by availability of the HA substrates UDP-glucosamine and UDP-glucuronic acid. KLF2 inhibits endothelial glycolysis and allows for glucose intermediates to shuttle into the hexosamine- and glucuronic acid biosynthesis pathways, as measured using NMR analysis in combination with ^{13}C labelled glucose.

Conclusions: These data demonstrate how endothelial glycocalyx function and functional adaptation to shear is coupled to KLF2 mediated regulation of endothelial glycolysis.

Introduction

The endothelium is covered by a glycocalyx surface layer, which consists of the polysaccharides heparan sulfate, hyaluronan and chondroitin sulfate [1, 2]. This layer confers most of the functional aspects of the endothelium. For example, specific sulfation patterns on heparan have been shown to be critical for engagement of growth factors and chemokines to their receptors and the function of surface bound proteins such as complement factor H and antithrombin III. In addition, this layer serves as barrier that governs capillary ultrafiltration. Finally, the glycocalyx layer transmits the shear forces of the flowing blood to the intracellular pathways that induce endothelial quiescence, such as KLF2. Conversely, altered shear forces have also been associated with changes in glycocalyx thickness [3, 4]. How the glycocalyx is synthesized and maintained to keep the endothelium in its quiescent state is unknown.

The main structural component of the endothelial glycocalyx is hyaluronan (HA). Hyaluronan is a very long polysaccharide that is synthesized at the inner surface of the plasma membrane from the substrates UDP-glucosamine (UDP-GlcNAc) and UDP-glucuronic acid (UDP-GlcA). HA is synthesized by the synthases HAS1, HAS2 or HAS3 and secreted into the extracellular space. These three isoforms differ in enzyme stability, elongation rate of HA and affinity of HA substrates [5], which potentially influences HA synthesis. HAS2 is the most widespread isoform correlated with HA distribution in mammals [6]. HAS2 knockout mice die early in gestation due to major defects in cardiovascular development, suggesting that HA may function as molecular platform for vascular signaling [7]. It is estimated that HAS2 polymerizes UDP-GlcA and UDP-GlcNAc at a rate of 20 monosaccharides/sec [5], rendering the synthesis critically dependent upon the cytosolic availability of these substrates.

UDP-GlcA and UDOP-GlcNAc are derived from respectively the glucuronic acid and hexosamine biosynthesis pathways. We therefore postulated that endothelial HA, and hence glycocalyx thickness, would depend upon endothelial glucose metabolism. It has been shown that in this respect endothelial cells are characterized by a high glycolytic flux, where the possibility for glucobiosynthesis can be postulated to be regulated by this flux. Interestingly, the shear stress responsive transcription factor KLF2 has been shown to inhibit PFKFB3 [8], the key enzyme that drives (hyper)glycolysis.

In this study we investigate the relationship and inter-dependency of shear adaptation, glucobiosynthesis and the ability to synthesize the glycocalyx layer, which is so critical for endothelial function.

Material and methods

Mice and Experimental groups

The details of the mice experiment has been descripted previously [9]. Given the implications found that gender differences exist in relation to volume regulation and exchange vascular homeostasis [10], only male mice were taken in this study to decrease the outcome variability. In brief, all experiments were performed using eight week old male (apoE−/−) mice on C57BL/6J background (Charles River), randomly divided into 4 groups. One group was fed a standard rodent diet (NC; Sniff R/M-H, Germany) for 6 weeks (n = 6). The other 3 groups of mice were put on a high fat-, high cholesterol diet containing 15% cacao butter, 0.25% cholesterol, 40.5% sucrose, 10% corn starch, 1% corn oil, and 5.95% cellulose (HFD; diet-W, Hope farms, the Netherlands) for 6 weeks. At the age of 14 weeks, 2 of the groups on HFD received an osmotic minipump and mouse jugular catheter (Alzet, Cupertino, CA) containing active- (n=6) or inactive (n=7) testicular hyaluronidase (bovine testis, Sigma-Aldrich). The mice were sacrificed under anaesthesia. All the mice were kept with ad libitum food and water in cages with bedding (Rehofix Corncob bedding MK1500, Technilab-BMI, Someren, the Netherlands) in a 12/12 hrs Light/dark cycle. The experimental protocol was approved by the local Animal Ethical Committee of Maastricht University (AEC protocol number 2007-031) and all animal work was performed in compliance with the Dutch government guidelines.

Cell isolation and culture

Human umbilical vein endothelial cells (HUVECs) were freshly isolated, by perfusion and subsequent incubation (20 minutes) of trypsin at 37 °C, from different donors as described [11] (with approval of the Medical Ethical Commission of the Leiden University Medical Center, and informed consent from all subjects) and used between passage 1 and 3. Freshly isolated HUVECs were cultured in 0.1% gelatine–coated plastic flasks in endothelial EGM2 (Lonza) medium, supplemented with human epidermal growth factor, vascular endothelial growth factor, human fibroblast growth factor-B, R3-IGF-I, ascorbic acid, heparin, and 10% human serum (CC-3121; Lonza, Basel, Switzerland), and with antibiotics/antimycotics (Life technology, Gibco), at 37 °C and 5% CO_2. HUVECs were treated with 1 mM UDP-GlcA (Sigma, U6751), 1 mM UDP-GlcNAc (Sigma, U4375) or 10 µM 3PO (Merck, 525330) for 72 hours, or treated with 100 µM 2DG (Sigma, D8375) for 24 hours. Cells were collected for further experimental assays.

In vitro flow experiments

HUVECs were cultured for 4 days at a constant laminar shear stress (10 dyne/cm^2) or an oscillatory shear stress (+/- 10 dyne/cm^2; 0.5Hz) in EGM2 (Lonza) using an ibidi flow system (Ibidi, Martinsried, Germany). Medium was refreshed after 1 day, non-adhered cells removed, and cultured under laminar

oscillatory flow for another three days at 37 °C and 5% CO_2. To test the effects of laminar versus oscillatory shear patterns, we used the same shear stress level of 10 dyne/cm^2 exposure for both the laminar- and the oscillatory flow groups. Such shear stress levels can also be found *in vivo* in disturbed /oscillatory conditions and have also been widely used in *in vitro* experimental setups to study the response shear [12, 13].

Neurocan-dsRed construct

The *N*-terminus rat neurocan construct of the hyaluronan specific neurocan-eGFP (Ncan-eGFP) construct [14], linked to the BM 40 signal peptide with APLGRGSHHHHHHGGLA and a GSSGA linker at the C-terminus, was excised and fused into a pDsRedMonoN1 (ClonTech, Mountain View, CA, USA) plasmid. The modified neurocan-dsRed (Ncan-dsRed) construct was incorporated into a self-inactivating (SIN) lentiviral vector (pLV-CMV-IE.Ncan-dsRed) and transduced into Hek293 cells. Supernatant was isolated and purified on a Ni-NTA resin column using the incorporated 6xHistidine tag within the protein.

Glycocalyx and HA staining

Deparaffinized mouse aorta sections (4 µm thick) were washed in PBS and antigen retrieval was performed in a citrate (pH 6.0) buffer in an autoclave. Slides were blocked in Serum-Free Protein Block buffer (Dako, Agilent Technologies Netherlands B.V., Amstelveen, the Netherlands) for 1 hour at room temperature. Ncan-dsRed was incubated overnight (at 4 °C) in HBSS (Gibco, 14175-053), followed by washing with HBSS and embedded in Prolong™ gold antifade mountant with DAPI (ThermoFisher, P36931).

Cells were fixed with 4% PFA in HBSS for 10 minutes at room temperature, washed in HBSS containing 1% BSA, and blocked for 30 minutes at room temperature in 5% BSA in HBSS. Ncan-dsRed or 10 µg/mL lectin from *Lycopersicon esculentum* (LEA, Sigma-Aldrich, L0401) were incubated overnight (at 4°C) together with Hoechst 33258 (Invitrogen™, H3569), followed by wash with 1% BSA in HBSS. Cells were examined using a LEICA TCS SP5 with a 100x objective (HCX PL APO CS 100x/1.40 oil, Leica). Sequential 16-bit confocal images (xyz dimensions, 0.142×0.142×0.3µm, 0.142×0.142×1µm or 0.116x0.116×1µm) were recorded using LAS-X Image software (Leica) and analysed with ImageJ. Surface glycocalyx and HA expression was quantified on 5 cells per field of view of 4 independent experiments, in essence as described earlier [15]. From a side-view, resliced from a line (10 pixels wide) over the nucleus 3 additional lines were drawn at the nuclear position and the mean fluorescence was calculated between the distance from half-maximum signal of the nuclear staining to half-maximum signal at the luminal end. Both thickness and average fluorescence were determined.

Immunofluorescence staining

Deparaffinized mouse aorta sections (4 µm thick) were washed in PBS and antigen retrieval was performed in a citrate (pH 6.0) buffer in an autoclave. Slides were blocked with 3% normal goat serum, 2% BSA and 0.01% Triton-X100 in PBS for 1 hour at room temperature. Primary anti-KLF2 antibody (abcam, ab203591), anti-mouse ICAM1 (Santa Cruz, sc-1511r) or rabbit IgG isotype control (abcam, ab172730) was incubated overnight (at 4°C), followed by Goat anti rabbit IgG AF488 for 1 hour. Slides were embedded in Prolong™ gold antifade mountant with DAPI (ThermoFisher, P36931).

Cells were fixed with 4% PFA in PBS for 10 minutes at room temperature, washed with PBS, and blocked for 1 hour at room temperature in block buffer (3% normal goat serum, 2% BSA and 0.3% triton in PBS). Anti-human CD144 (BD bioscience, 6273648), Phalloidin-Tetramethylrhodamine B isothiocyanate (Sigma, P1951) and Hoechst 33258 (Invitrogen™, H3569) were incubated overnight (at 4°C), followed by wash with PBS. Then incubate with Goat anti mouse IgG1 AF488 for 1 hour at room temperature and wash with PBS.

RNA isolation and RT-PCR

Cells were harvested in Trizol reagent (Life Technologies, 15596018). Total RNA was isolated using RNeasy mini kit (Qiagen, 74106) according to its protocol. cDNA was synthesized by mixing 1 mg total RNA, Oligo (dT) (Promega, C110A) and dNTP (Promega, C110A) and incubate at 65 °C for 5 minutes firstly. Then M-MLV reverse transcriptase (Promega, M170B), recombinant RNasin® ribonuclease inhibitor (Promega, N251B) and DTT were added into the mixture and incubate at 37 °C for 50 minutes. terminate the reaction by incubating at 70 °C for 15 minutes. SYBR select master mix (Applied Biosystems™, 4472897) and specific primers (supplementary table I) was used for real time PCR. The expression of genes were determined by normalized to GAPDH levels.

Virus transduction

The HAS2 and HAS3 short-hairpin RNA lentiviral constructs (pLV-CMV-IE.HAS2shRNA, pLV-CMV-IE.HAS3shRNA) were created through transfecting Hek293 cells (20-40% confluence) with a mixture of combined plasmid DNA of Has2shRNA (Sigma-Aldrich, Mission shRNA library #9868) or Has3shRNA (Sigma-Aldrich, Mission shRNA library #9903), H1/VSVG and H23/pspax2 with polyethylenimine (PEI, 0.05 mg/mL final concentration) in DMEM (Gibco) to obtain the self-inactivating (SIN) lentiviral construct from supernatant, in principle as described [16]. Primary HUVEC were cultured to 60-80% confluency in T75 flasks (Greiner bio-one, Alphen a/d Rijn, the Netherlands) in EGM2 medium and transduced with pLV-CMV-IE.HAS2shRNA, HAS3shRNA or control (pLV-CMV-IE) in combination with 8 µg/mL polybrene, incubated o/n at 37°C and 5% CO2. After medium refreshment incubated for another 48 hours before collecting for experimental assays.

To induce a transient constitutive high expression of HAS2 and production of hyaluronan, the human *HAS2/pIRES-2-eGFP* [17] construct (gift from J.B. McCarthy) was transferred into pShuttle*CMV-Luciferase* to create the adenoviral vector Ad5*CMV-HAS2*, adenoviral control is Ad5*CMV-Luciferase.* [18]. For infection of HUVECs with the adenoviral constructs, cells were cultured to 60-80% confluency. 2MOI virus in combination with 8 µg/mL polybrene in EGM2 medium were added into the cells and incubate o/n at 37 °C and 5% CO_2. After medium refreshment incubated for another 24 hrs before collecting for experimental assays.

Glycolytic flux measurement

HUVECs were seeded overnight at 6×10^4 cells per well on fibronectin (Sigma) coated Seahorse XF96 polystyrene tissue culture plates (Seahorse Bioscience). The plate was incubated in unbuffered DMEM assay medium (Sigma) for 1 hour in a non-CO_2 incubator at 37 °C before measuring in an XFe 96 extracellular flux analyser (Seahorse Bioscience). Extracellular acidification rate (ECAR) were measured over 4 min periods with a mixing of 2 minutes in each cycle, with five cycles in total. Inhibitors and activators were used at the following concentrations: Glucose (5 mM), Oligomycin (5 µM) and 2-DG (100 mM). Cellular protein content was determined with a BCA-protein kit from Pierce (Thermo-Fischer Scientific) and the data is represented as ECAR normalized to protein.

Metabolites measurement

Quantitative analysis of intracellular and extracellular metabolites in *in vitro* EC cultures were performed using NMR spectroscopy as described in detail elsewhere [19, 20]. Briefly, MOCK and *KLF2*^{OE} ECs in triplicates were washed with warm PBS (37 °C) to remove the culture medium and quickly quenched with liquid nitrogen to arrest metabolism. The cells were subsequently scraped of the plates and extracted using a cold (-80°C) solution of methanol/chloroform/water, 8.1:0.9:1 (*v*/*v*/*v*). After leaving the samples on dry ice for 30 minutes, the extracts were centrifuged for 20 min at 18,000 × *g*, at 4 °C.

Prior to washing ECs with PBS, 0.2 mL of culture medium was collected from each sample and mixed with 0.4 mL of cold (-80 °C) 100% LC-grade methanol to extract extracellular metabolites. All samples were subsequently placed at -80°C for at least 30 minutes and centrifuged for 20 minutes at 18,000 × *g*, at 4 °C.

The supernatants from both cell extracts and culture medium extracts were collected and dried with nitrogen gas. NMR samples of extracts were prepared by dissolving the dried material with 0.22 mL of 0.15 M phosphate buffer (pH 7.4) in deuterated water containing 0.05 mM trimethylsilyl propionic-*d*4-sodium salt (TSP-*d*4) as internal standard for NMR referencing and quantification. An 1D ^{1}H-NMR spectrum was collected for each sample on a 14.1 T (600 MHz for ^{1}H) Bruker Avance II NMR, using the

1D-NOESY experiment with presaturation as implemented in the spectrometer library (Topspin v3.0, pulse sequence: *noesygppr1d*; Bruker Biospin, Ltd). All spectra were processed to correct the phase and baseline and imported in Chenomx NMR suite 8.4 (Chenomx NMR suite, v8.0, Edmonton, Canada) for quantification of metabolites. The protein bullet was dissolved in lysis buffer (150 mM NaCl, 1% SDS, 0.5% deoxycholate and 0.5% triton X-100, pH 7.5) with sonification. The protein concentration was measured using Pierce™ BCA protein assay kit (ThermoFisher, 23225) according to its manual. All concentrations were normalised to the total protein mass of each sample.

For ^{13}C fractional enrichment analysis, triplicates of MOCK and *KLF2*^{OE} were cultured in glucose-free medium, enriched by 5 mM U-$^{13}C_6$-D-Glucose and processed as described above. Fractional enrichment was calculated as described elsewhere[20] by deconvoluting and quantifying the protons at 5.52, 5.60 and 5.62 ppm (from UDP-GlcNAc, UDP-Glc, and UDP-GlcA, respectively), the protons at 5.99-6.03 ppm (overlapped peaks from all 3 sugars) and the protons at 7.9 ppm (overlapped peaks from all 3 sugars).

HA size analysis

For HA size analysis, we used the online protocol from Cleveland Clinics (NHLBI # PO1HL107147). HUVECs were digested with proteinase K solution (0.1 mg/mL proteinase K (Promega, V302B), 0.001% SDS, 100 mM ammonium acetate, pH 7.0) for 4 hours at 60 °C. Samples were precipitated and washed with cold ethanol. Nucleic acid was digested with benzonase nuclease (Sigma, E1014) at 60 °C overnight and enzyme was inactivated in a boiling water bath for 5 minutes. Samples were precipitated and washed with cold ethanol again. Samples were resuspended in 10 M formamide and loaded in a 0.5 cm thick 1% agarose gel and run for 1.5 hours. Finally, the gel was stained with stain-all (Sigma, E9379) solution and imaged with a camera.

CRISPR Cas9 editing

Experiments were performed using the Alt-R® CRISPR-Cas9 system (Integrated DNA technologies, IDT, USA) according to manufacturers' user guide. Guide RNA (gRNA, TGACTGCAAACGTCAAAACATGG) specific targeted to the HAS2 c-terminal was designed and gRNA containing crRNA was synthesised by IDT. A crRNA:tracrRNA duplex was formed by incubating two synthetic modified RNAs (crRNA and tracrRNA) at 95 °C for 5 minutes. Ribonucleoprotein complexes (RNP) were formed by incubating crRNA:tracrRNA duplex and Alt-R® S.p. Cas9 nuclease (IDT, 1081060) at room temperature for 20 minutes. A single-stranded oligodeoxynucleotide (ssODN) repair template contained a small tetracysteine tag (TC-tag, Cys-Cys-Pro-Gly-Cys-Cys, GGACAACAATATGACATGGTGCTTGATGTATGTTG TCCTGGCTGTTGTTGATCTTCTATGTTTTGACGTTTGCAGTCACACACAACACCTT) was synthesised by IDT.

RNP and ssODN were co-deliveried into HUVECs using Amaxa® HUVEC nucleofector® kit (Lonza, VPB-1002) according to its manual.

HAS2-TC imaging

Cells were gently washed with prewarmed (37 °C) HBSS and immerse with 2 µM FlAsH-EDT_2 (Cayman, 20704) in prewarmed HBSS and 10 µM 1,2-ethanedithiol (EDT) at 37 °C for 30 minutes. Aspirate FlAsH-EDT_2 solution from cells and replaced with 250 µM 2,3-dimercaptopropanol (BAL) in HBSS at 37 °C for 15 minutes. Wash solution was removed and replaced with prewarmed HBSS. HAS2-TC positive cells was imaged on a LEICA SP8 WLL confocal microscope. Sequential 16-bit confocal images (xyz dimensions, 0.142×0.142×0.3µm) were recorded and 3D images were rendered using LAS-X Image software (Leica). The total stained area of each cell was analysed using ImageJ software.

Immunoblotting

Western blots were performed form protein extracts of HUVECS. Cells were washed with PBS and lysed in 50mM TRIS HCL buffer (pH 7.5) containing 150mM NaCl, 1% SDS, 0.5% deoxycholate and 0.5% triton X-100. Protein samples were diluted 5x in SDS sample buffer (pH 6.8; 10% SDS, 25% 2-mercaptoethanol, 50% glycerol, 0.01% bromophenol blue, 0.3125M Tris-HCl, 0.5M DTT), incubated at 95°C for 10 minutes and subjected to SDS-PAGE and western blotting. Proteins, transferred to PVDF membrane (1704156, Bio-Rad Laboratories BV, Veenendaal, The Netherlands) were detected with antibodies against GAPDH (MA5-15738, ThermoFisher) and ICAM1 (4915s, Cell signaling technology), after blocking the membrane with 5% fat-free milk in PBS and 0.1% Tween-20. Followed by incubation with a secondary HRP-conjugated antibody and Pierce ECL Western Blotting substrate (32106, Thermo Scientific). Band intensity was analysed using ImageJ software. For the HAS2 protein expression detection, protein samples together with antibodies against HAS2 (sc-34067, Satan Cruz) or GAPDH (MA5-15738, ThermoFisher) were applied in WES machine (Proteinsimples, California, USA). The protein expression was measured based on the intensity of peaks given by WES, and a representative digital band was shown.

Statistical analysis

Data are presented as mean ± SD, unless indicated otherwise. For all experiments, 3-5 biological replicates were performed. All data were performed with Shapiro-Wilk test and Levene's test to evaluated the normality and variances firstly. For the normally distributed and equal variance data, the differences between two groups were assessed by paired 2-tailed Student's t test, and between multiple groups were assessed by one-way ANOVA followed by Tukey test. P values < 0.05 were considered statistically significant. If the data were not normally distributed or not of equal variance, the Mann-Whitney *U* test was performed. P values < 0.05 were considered statistically significant.

Results

Laminar shear stress induces surface HA production through increased hyaluronan synthase 2 expression

Shear stress plays a crucial role in glycocalyx modeling and endothelial integrity. To test the glycocalyx HA expression upon the atheroprotective- or atheroprone shear stress *in vivo*, a specific HA binding peptide (Ncan-dsRed) was used to stain HA in mouse aorta. Endothelial cells exposed to laminar shear stress showed a higher HA expression than the endothelial cells at lesion prone sites exposed to disturbed shear stress in apoE-KO mouse aorta which revealed a higher ICAM1 expression (figure 1A-D). To explore the role of endothelial HA in the progress of atherosclerosis, ApoE-KO mice at a high-fat diet were studied. At the lesion sites exposed to disturbed shear stress, endothelial HA was diminished and instead increased ICAM1 expression was observed (supplementary figure I A-C). Furthermore, endothelial HA removal by chronic infusion with active hyaluronidase in ApoE-KO mice on HFD (supplementary figure I D and E), showed further loss of HA in the disturbed shear stress region and resulted in formation of advanced lesions with increased matrix deposition. [9] Also, in the laminar shear stress regions increased ICAM1 expression was observed (supplementary figure I F and G), which suggested that endothelial cells are activated after loss of luminal surface HA despite the presence of laminar shear.

An Ibidi flow system was also used to culture endothelial cells *in vitro*. As reported earlier [21], we observed that prolonged laminar shear stress (4-7 days at 10 dyne/cm^2) exposure aligned HUVECs into the direction of flow, increased localization of VE-cadherin at the cell borders and decreased F-actin stress fibers (supplementary figure II A). We next tested the luminal glycocalyx layer expression of ECs in response to shear stress. Four days of exposure to 10 dyne/cm^2 laminar shear stress induces a maximum total intensity of lectin from *Lycopersicon esculentum* (LEA) binding, which is significantly increased in comparison to static culture or 4-days of oscillatory shear (supplementary figure S2B and C). In addition, increased endothelial surface HA expression was also found after 4-days of laminar shear, in comparison to exposure of oscillatory shear or static cultured EC, when stained with Ncan-dsRed (figure 1E-G, supplementary figure II D-F). In line with the observed HA production, laminar shear stress induced HAS2 protein expression (figure 1H and I). Gene expression analysis revealed that exposure to prolonged laminar shear increased *HAS2* (figure 1J) while *HAS3* was decreased (figure 1K), *HAS1* expression was undetectable (data not shown).

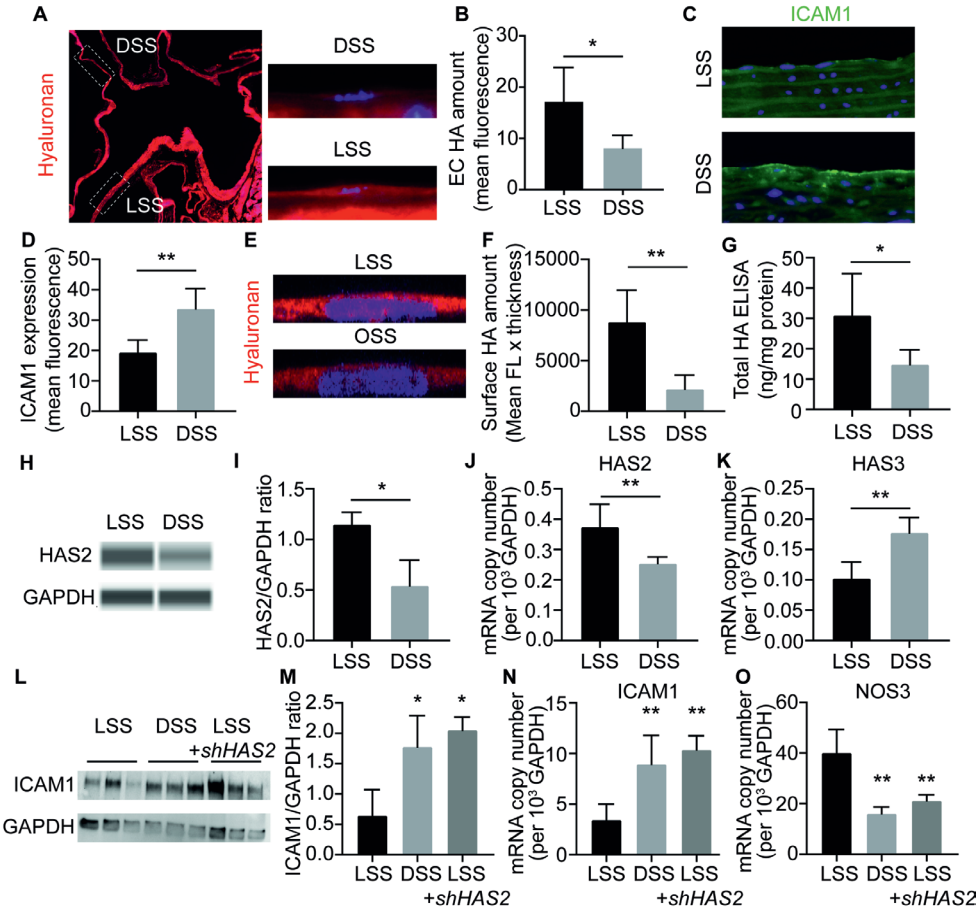

Figure 1. Laminar shear stress is associated with increased endothelial HA and HAS2 expression. (A) Representative images of HA stained at the surface within the aortic arch region of *apoE*-KO mice on standard diet (n=6). Areas exposed to laminar shear stress (LSS) or disturbed shear stress (DSS) are labelled with Ncan-dsRed, and demonstrate preferential luminal presence of HA in LSS exposed regions. (B) Quantification of HA staining in LSS and DSS exposed aortic regions. (C) Representative images of ICAM1 staining of the aortic regions exposed to LSS and DSS and (D) Quantification. (E) Representative confocal images of HA staining of HUVECs after 4 days LSS, or after 4 days exposure to oscillatory shear stress (OSS), respectively. (F) Quantification of endothelial surface HA under different culture conditions, presented as mean fluorescence times thickness (mean FL x thickness). (G) Quantification of total endothelial HApresence. (H) Representative WB images of endothelial HAS2 protein expression and (I) quantification. (J) HAS2- and (K) HAS3 mRNA expression in response to LSS or OSS, normalized to 10^3 copies GAPDH. (L) WB images of ICAM1 protein expression and (M) quantification in HUVECs after knockdown of HAS2 (*shHAS2*) or mock virus as control after 4 days of

LSS or OSS exposure. (N) ICAM1- and (K) NOS3 mRNA expression under different culture conditions, normalized to 10^3 copies GAPDH. All values are given as mean ± SD of 3-7 independent experiments. Non-paired 2-tailed Student's t test and one-way ANOVA followed by Tukey test were performed; *P < 0.05, **P < 0.01.

To further corroborate the requirement of HAS2 in endothelial HA production, we cultured HUVECs after silencing *HAS2* or *HAS3* gene expression with a lentiviral shRNA construct (supplementary figure III A). Although normal *HAS2* gene expression was lower than *HAS3* in static cultured HUVECs, only silencing of HAS2 (*shHAS2*) significantly decreased surface HA expression, -production and -HMW HA content, while *shHAS3* had no effect (supplementary figure III B-D). Moreover, *shHAS2* blocked the laminar shear stress induced athero-protective role by increasing *ICAM1* expression (figure 1L-N) and decreasing *NOS3* expression (figure 1O). Overexpression of *HAS2* (*HAS2^{OE}*) in turn, resulted in a strong increase of cellular HMW HA content and surface HA (supplementary figure III D-F). However, *HAS2^{OE}* also increased LMW HA content (supplementary figure III D) and intracellular HA production (supplementary figure III E), both possible pro-inflammatory factors [22, 23]. These data suggests a strict regulation of endothelial HA production in order to keep cellular integrity.

Shear stress induces HAS2 protein amount and translocation to the endothelial apical membrane

HA is synthesized by its synthases at the inner face of the plasma membrane and secreted into the extracellular space. To detect the expression and location of HAS2 protein under shear stress, we inserted a small tetracysteine tag (TC-tag, Cys-Cys-Pro-Gly-Cys-Cys) into the C-terminal end of the HAS2 gene (figure 2A), using co-delivery of Cas9 protein pre-complexed with two synthetic modified RNAs (crRNA and tracrRNA) and a single-stranded oligodeoxynucleotide (ssODN) repair template in HUVEC (figure 2B). After conformation of the knock-in (figure 2C and supplementary figure IV A), the efficiency was determined to be about 2.5% without selection (figure 2D). Static EC cultures revealed a very low amount of intracellular TC-tagged HAS2 protein after introducing FlAsH-EDT2 labelling reagent (figure 2E), while TGFβ treatment, as a positive control, induced HAS2 expression (supplementary figure IV B and C). When endothelial cells are exposed to laminar shear stress for four days, not only the intracellular amount of HAS2 protein increases but translocation of HAS2 to the apical membrane could also be observed compared to exposure to oscillatory shear stress or static culture (figure 2E and F).

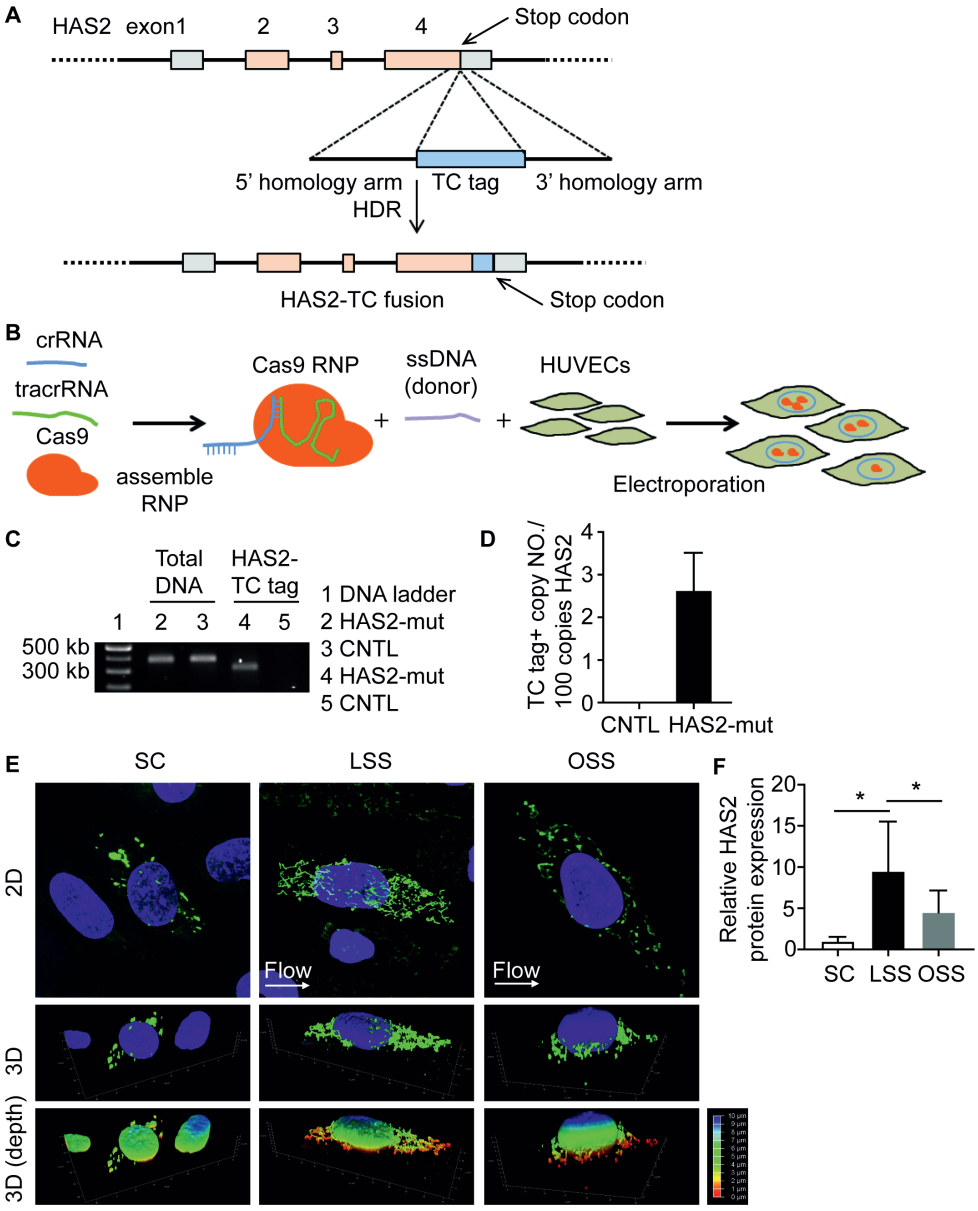

Figure 2. Laminar shear stress induces HAS2 protein amount and translocation to the endothelial apical membrane. (A) A small tetracysteine tag (TC-tag, Cys-Cys-Pro-Gly-Cys-Cys) was inserted into the C-terminal end of the *HAS2* gene using (B) co-delivery of Cas9 protein pre-complexed with two synthetic modified RNAs (crRNA and tracrRNA) and a single-stranded oligodeoxynucleotide (ssODN) repair template in HUVEC. (C) Identification of the *HAS2*-TC-tag fusion using PCR and determination of (D) efficiency of the knock-in. (E) Representative images of HAS2-TC-tag protein expression in static

culture (SC), LSS and OSS. HAS2-TC tag visualized in 2D (top row), 3D (middle row) and 3D (depth color coding; bottom row). (F) Quantification of HAS2-TC-tag protein expression, presented as relative to static culture. A total of 12 cells from each group were imaged and quantified. All values are given as mean ± SD. Non-paired 2-tailed Student's t test and one-way ANOVA followed by Tukey test were performed; *P < 0.05.

Endothelial Krüppel-like factor 2 increases surface HA expression

Endothelial cells exposed to laminar shear stress showed a higher KLF2 expression than exposure to disturbed shear stress in mouse aorta (figure 3A and B). *In vitro*, only prolonged laminar shear stress induces endothelial KLF2 gene expression (figure 3C). A highly conserved KLF2 binding domain CACCC box [24, 25] was found in the *HAS2* promoter region (figure 3D), which is a potentially transcriptional regulator of *HAS2* expression. To test a possible link between endothelial *KLF2* expression and hyaluronan production, we used a lentiviral KLF2 construct to increase KLF2 ($KLF2^{OE}$) in HUVECs. As expected, $KLF2^{OE}$ significantly increased both HAS2 mRNA and protein expression (figure 3E-G). In line with laminar shear stress exposure, KLF2 overexpression also resulted in increased HA expression (figure 3H-I and supplementary figure V A). Moreover, inhibition of KLF2 expression blocked the laminar shear stress induced HAS2 expression and HA production (figure J-M).

HAS2 responsible HA synthesis in endothelial cells is dependent on substrate availability

In contrast to synthesis of the other glycosaminoglycans, which takes place in the Golgi system, HA is produced at the plasma membrane using the cytoplasmic substrate pool. Therefore, cytosolic availability of UDP-GlcA and UDP-GlcNAc can be postulated to be critical for this process, rendering the metabolic state of the cell an important factor for production of HA[26-30]. Increasing extracellular concentrations of UDP-GlcA and UDP-GlcNAc in the medium, both resulted in increased HA production in a HAS2 dependent manner (figure 4A-D), especially UDP-GlcA, indicating that cellular availability of substrates determines HA production.

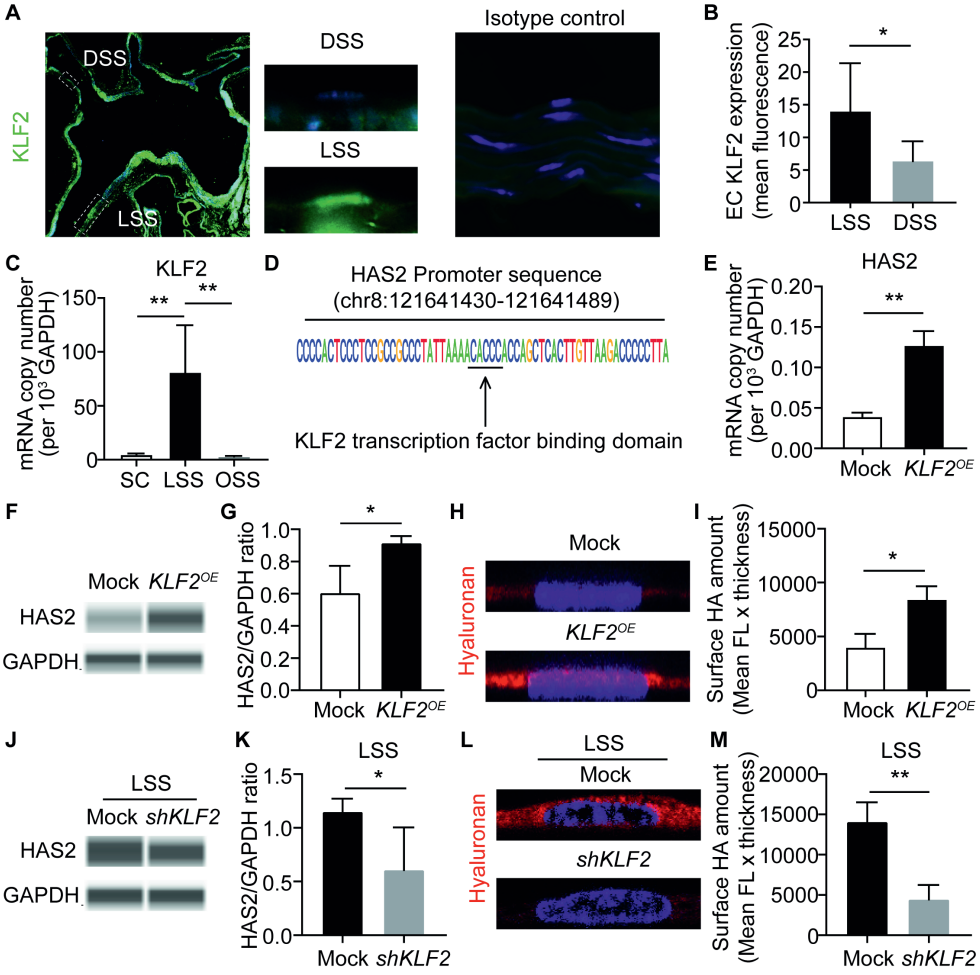

Figure 3. Laminar shear stress induces HA production by increased KLF2 expression and KLF2 mediated HAS2 expression. (A) Representative images of KLF2 staining in the aortic arch region of *apoE*-KO mice on standard diet (n=6). Areas exposed to laminar shear stress (LSS) or disturbed shear stress (DSS) are labelled respectively. Rabbit IgG was used as an isotype control of KLF2 staining. (B) Quantification of KLF2 protein expression. (C) KLF2 mRNA expression in HUVECs exposed to LSS or OSS. (D) Highly conserved KLF2 binding domain "CACCC" as found in HAS2 promoter region. (E) HAS2 mRNA expression in response to *KLF2* overexpression (*KLF2*^{OE}), normalized to 10^3 copies *GAPDH*. (F) Representative WB images of endothelial HAS2 protein expression and (G) quantification in response to *KLF2*^{OE}. (H) Representative confocal images of HA staining in HUVECs upon *KLF2*^{OE} with (I) quantification of surface HA. (J) Representative WB images of endothelial HAS2 protein expression and (K) quantification after knockdown of *KLF2* (*shKLF2*) exposed to LSS. (L) Representative confocal

images of HA staining in HUVECs upon *shKLF2* exposed to LSS with (M) quantification of surface HA. All values are given as mean ± SD of 3-7 independent experiments. Non-paired 2-tailed Student's t test and one-way ANOVA followed by Tukey test were performed; *P < 0.05, **P < 0.01.

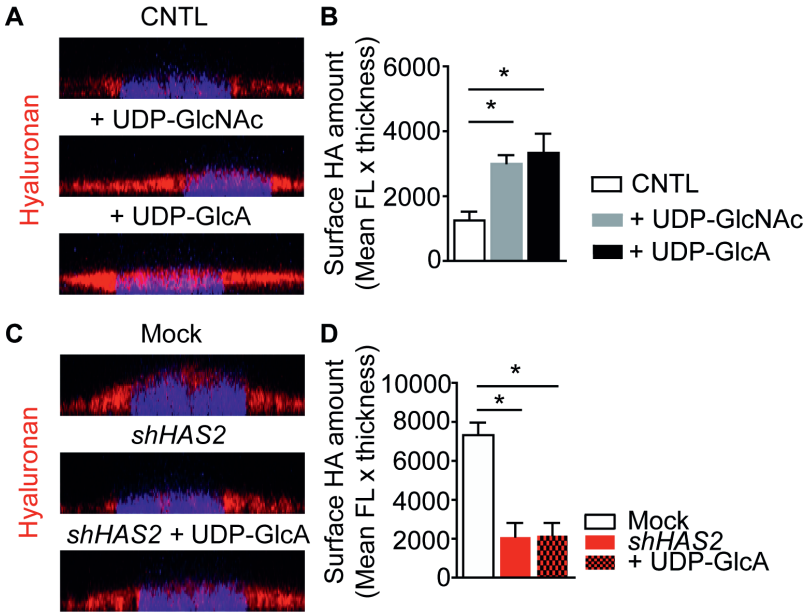

Figure 4. HA synthesis by HAS2 in endothelial cells is dependent on substrate availability. (A) Representative confocal images of HA staining and (B) quantification of endothelial surface HA on HUVECs in the presence of 1 mM UDP-GlcA or 1 mM UDP-GlcNAc for 72hrs. (C) Representative confocal images of HA staining and (D) quantification of surface HA on HUVECs after knock-down of HAS2 (*shHAS2*), in presence of 1 mM UDP-GlcA for 72hrs. All values are given as mean ± SD of 3-4 independent experiments. Non-paired 2-tailed Student's t test and one-way ANOVA followed by Tukey test were performed; *P < 0.05.

KLF2 induces intracellular UDP-sugar flux through regulating glucose usage

To test the critical cytosolic availability of UDP-GlcA and UDP-GlcNAc for HA biosynthesis in response to shear stress, we investigated substrate availability in relation to the endothelial metabolic state with $KLF2^{OE}$. Prolonged laminar shear repressed gene expression of the glycolytic activator *PFKFB3* through KLF2 activation(figure 5A-C). Measuring the extracellular acidification rate (ECAR), as an indicator of lactate production, showed reduced glucose-induced glycolysis and maximal glycolytic capacity, defined as ECAR induced by the mitochondrial respiration blocker oligomycin to force the cells to rely more on glycolysis after *KLF2* overexpression of ECs (supplementary figure V B).

To test how this change in glycolytic rate influences the HAS2 substrate availability, we used ^{13}C labelled glucose in combination with nuclear magnetic resonance (NMR) analysis to determine the intracellular fate of glucose derived metabolites. *KLF2*^{OE} in ECs resulted in a reduced glucose uptake rate (figure 5D) and lactate release rate (figure 5E), consistent with the Seahorse data. The intracellular ^{13}C-glucose amount was significantly increased upon *KLF2*^{OE} (figure 5F), however, without changes in relative ^{13}C enrichment of intracellular glucose (figure 5G, top row), which remains above 90%. This demonstrates that intracellular ^{12}C-glucose was efficiently and proportionally replaced by ^{13}C-glucose. When measuring subsequently the ^{13}C-labelled glucose ring of the UDP-sugars which part will be incorporated into HA (supplementary figure V C), *KLF2*^{OE} increased the concentrations of UDP-Glc, UDP-GlcA and UDP-GlcNAc (figure 5H-J). Moreover, fractional ^{13}C enrichment in the UDP-sugar glucose ring was also increased in *KLF2*^{OE} ECs while ^{13}C labeled glucose was unchanged (figure 5G), thus demonstrating induction of glucose flux into the UDP-sugars biosynthesis (figure 5K). As expected, the fractional enrichment of the ^{13}C-labelled ribose ring of the UDP-sugars, which will be released into the cytosol as UDP and potentially reused as synthetic precursor of UDP-sugars, did not change (supplementary figure V D-G), suggesting the flux of glucose derived from UTP into UDP-sugars remains the same. In summary, reduced glycolysis upon *KLF2*^{OE} in ECs resulted in a higher glucose flux into the UDP-GlcA and UDP-GlcNAc biosynthesis pathways (figure 5K). In agreement, we observed reduced endothelial HA surface expression after knock-down of the key regulatory enzymes UDP-glucose pyrophosphorylase 2 (*UGP2*), UDP-glucose dehydrogenase (*UGDH*) or fructose amidotransferase 1 (*GFPT1*) in ECs exposed to laminar shear stress (figure 5L and M) or in static culture without changing *HAS2* gene expression (supplementary figure VI A-C).

Inhibition of glycolysis by 3PO increases HA production

To confirm that the change of glycolytic rate influences HA biosynthesis, we used the pharmacologic PFKFB3 inhibitor 3PO to decrease glycolysis in HUVECs. An increase of HA expression upon 3PO treatment was observed in ECs in static conditions in a HAS2 dependent manner (figure 6A-C), while 3PO treatment did not change the HAS2- or 3 expression itself (figure 6D and 6E). Inhibition of glycolysis with a low dose of 2DG also increased HA production under static culture (figure 6H). The same effect of 3PO treatment on HA production was also shown in ECs exposed to oscillatory shear stress (figure 6F). However, these effects were no longer detected when ECs were exposed to laminar shear stress (10 dyne/cm^2) (figure 6G).

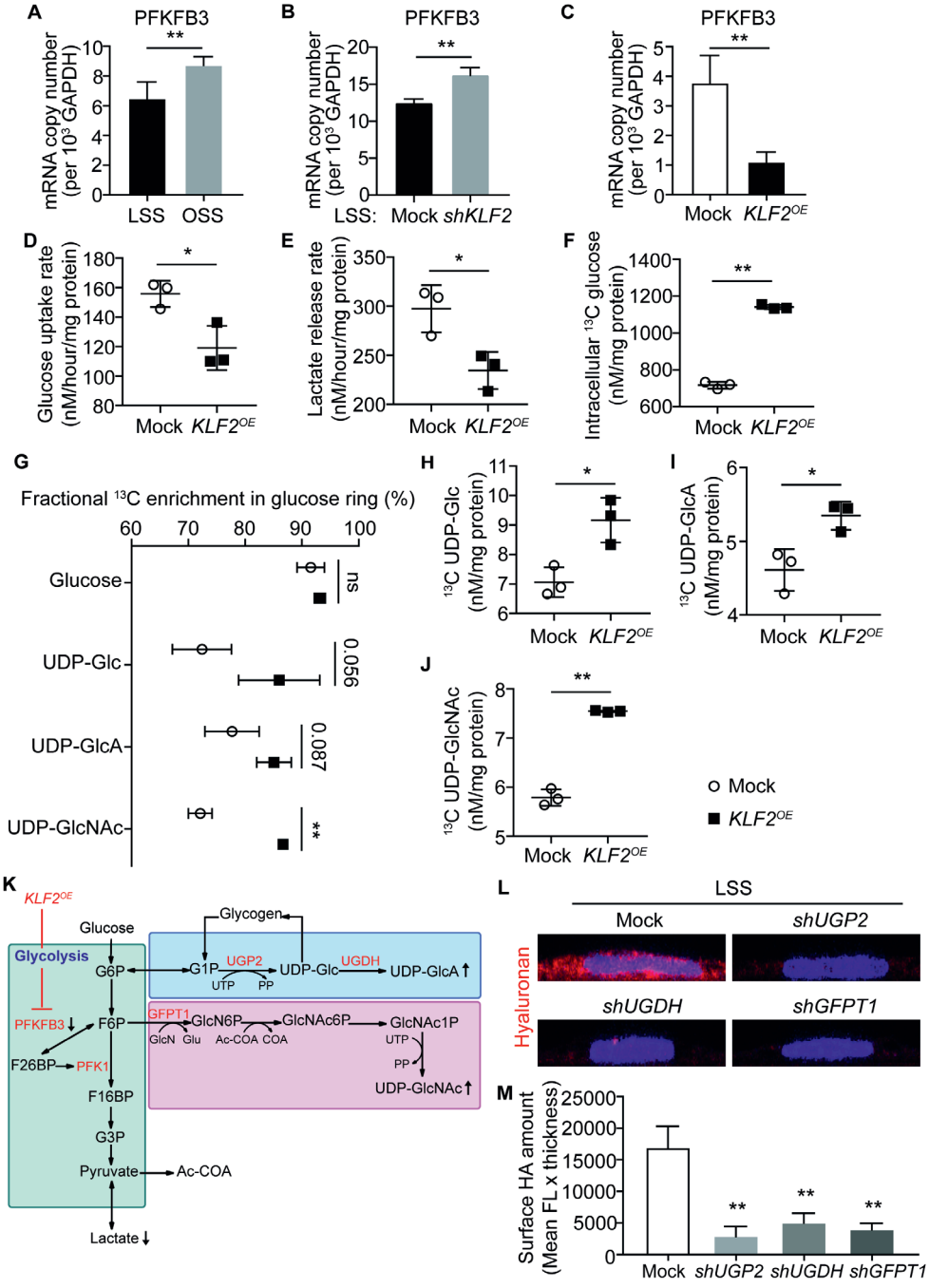

Figure 5. *KLF2* increases intracellular HA substrate availability and HA synthesis by shuttling UDP-sugar flux to the hexosamine- and glucuronic acid biosynthesis pathways. (A) PFKFB3 mRNA expression in HUVECs exposed to LSS or OSS. (B) PFKFB3 mRNA expression in HUVECs upon *shKLF2*

exposed to LSS. (C) PFKFB3 mRNA expression in HUVECs in response to *KLF2*^{OE}. Changes in intracellular and extracellular UDP-sugar metabolite concentrations are measured using NMR of ^{13}C-glucose over ^{12}C-glucose incorporation. (D) Glucose uptake rate and (E) lactate release rate were quantified based on extracellular tracer concentrations before and after 24hrs culture. (F) Intracellular ^{13}C glucose quantification change upon *KLF2*^{OE}. (G) Enrichment analysis of the UDP-sugar ^{13}C labeled glucose ring as measure of ^{13}C flux change of UDP-sugars. Quantification of intracellular UDP-sugar metabolite measurements using the ^{13}C labeled glucose ring of (H) UDP-Glc, (I) UDP-GlcA and (J) UDP-GlcNAc. (K) Pathway map of changed glucose usage through glycolysis and its side branches for UDP-sugars biosynthesis upon *KLF2*^{OE}. (L) Representative confocal images of HA staining in HUVECs after knockdown of the key rate-limiting enzymes UDP-glucose pyrophosphorylase 2 (*shUGP2*), UDP-glucose dehydrogenase (*shUGDH*), or glutamine-fructose-6-phosphate transaminase 1 (*shGFPT1*), after 4 days of LSS exposure, and (M) quantification of surface HA. All values are given as mean ± SD of 3-7 independent experiments. Non-paired 2-tailed Student's t test and one-way ANOVA followed by Tukey test were performed; *P < 0.05, **P < 0.01.

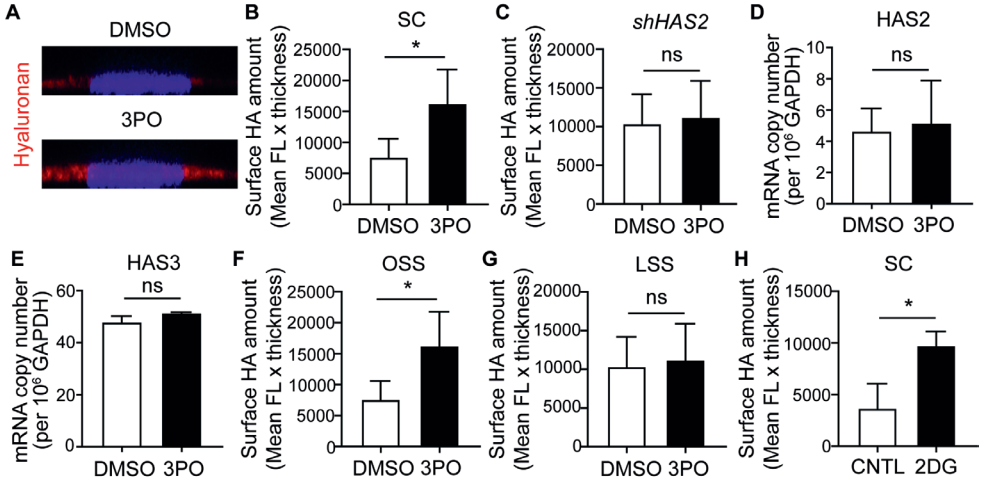

Figure 6. Inhibition of PFKFB3 by 3PO increases HA production. (A) Representative confocal images of HA staining of HUVECs with PFKFB3 inhibitor (3PO) or DMSO as control under SC. Quantification of surface HA on HUVECs with 3PO treatment (B) under SC or (C) after knock-down of HAS2 under SC. (D HAS2- and (E) HAS3 mRNA expression in response to 3PO under SC, normalized to 10^6 copies GAPDH. Quantification of surface HA on HUVECs with 3PO treatment (F) exposed to OSS or (G) LSS. (H) Quantification of surface HA on HUVECs with 2-Deoxy-D-glucose (2DG) treatment under SC. All values are given as mean ± SD of 3-4 independent experiments. Non-paired 2-tailed Student's t test was performed; *P < 0.05.

Discussion

The current study demonstrates how endothelial cell adaptation to alterations in shear stress through KLF2 is coupled to glycolytic flux (figure 7A and B). We show that the endothelial glycolytic flux determines the availability of the cytosolic substrates UDP-GlcNAc and UDP-GlcA and that these are rate limiting to synthesis of the endothelial glycocalyx component hyaluronan. Consequently, KLF2 mediated suppression of glycolysis results in a thicker glycocalyx layer. Moreover, laminar shear is also accompanied by KLF2 dependent increase in synthesis and membrane localization of the HA producing enzyme HAS2, which in quiescent EC appears to be the main HA producing enzyme.

The endothelial glycocalyx is critically involved in vascular integrity and homeostasis. Loss of this structure is associated with endothelial activation and dysfunction [31-33]. Hyaluronan in the glycocalyx has also been demonstrated to modulate inflammatory processes. The HMW form of hyaluronan possesses anti-inflammatory, anti-angiogenic, and immunosuppressive properties and protects cells from injury, and leukocyte adhesion [34]. In part this is related to its gel-like physical properties that preclude direct contact of leukocytes with the endothelial surface. In addition, HA can modulate growth factor and chemokine gradients at the endothelial surface. For example, binding of tumor necrosis factor (TNF)-stimulated gene 6 (TSG-6) to hyaluronan inhibits chemokine-stimulated trans-endothelial migration of neutrophils via a direct interaction between TSG-6 and the glycosaminoglycan-binding site of CXCL8 [35]. HA was also shown to mediate angiopoietin 1 binding to its endothelial TIE2 receptor, thus constituting a cell surface matrix that regulates EC-pericyte cross communication [36]. We recently corroborated the *in vivo* relevance of HA for endothelial glycocalyx function using an inducible endothelial deletion mouse model of Has2. Gene inactivation resulted in loss of glycocalyx structure, capillary destabilization, loss of endothelial barrier function and endothelial activation, and consequently in organ damage [36].

Endothelial adaptation to shear is known to be a biphasic process [37-39]. In the early phase (first hours), inflammatory signaling dominates and result in endothelial cell activation [38, 39]. This inflammatory signaling may also activate HAS2 and HA synthesis [38-41]. However, HA polymerization in these conditions may lead to HA cable formation and contribute to inflammatory vascular remodeling [23]. After days of sustained laminar shear, the endothelial cells become quiescent after downregulation of its inflammatory pathways (supplementary figure S2I). Interestingly, as we show, this is again a stimulus for HA synthesis. This time it is KLF2 mediated, where HAS2 translocation and metabolic availability of the UDP-sugars that serve as substrate for HA polymerization are co-regulated. We show that this co-regulation is a critical step to endothelial glycocalyx presence and function.

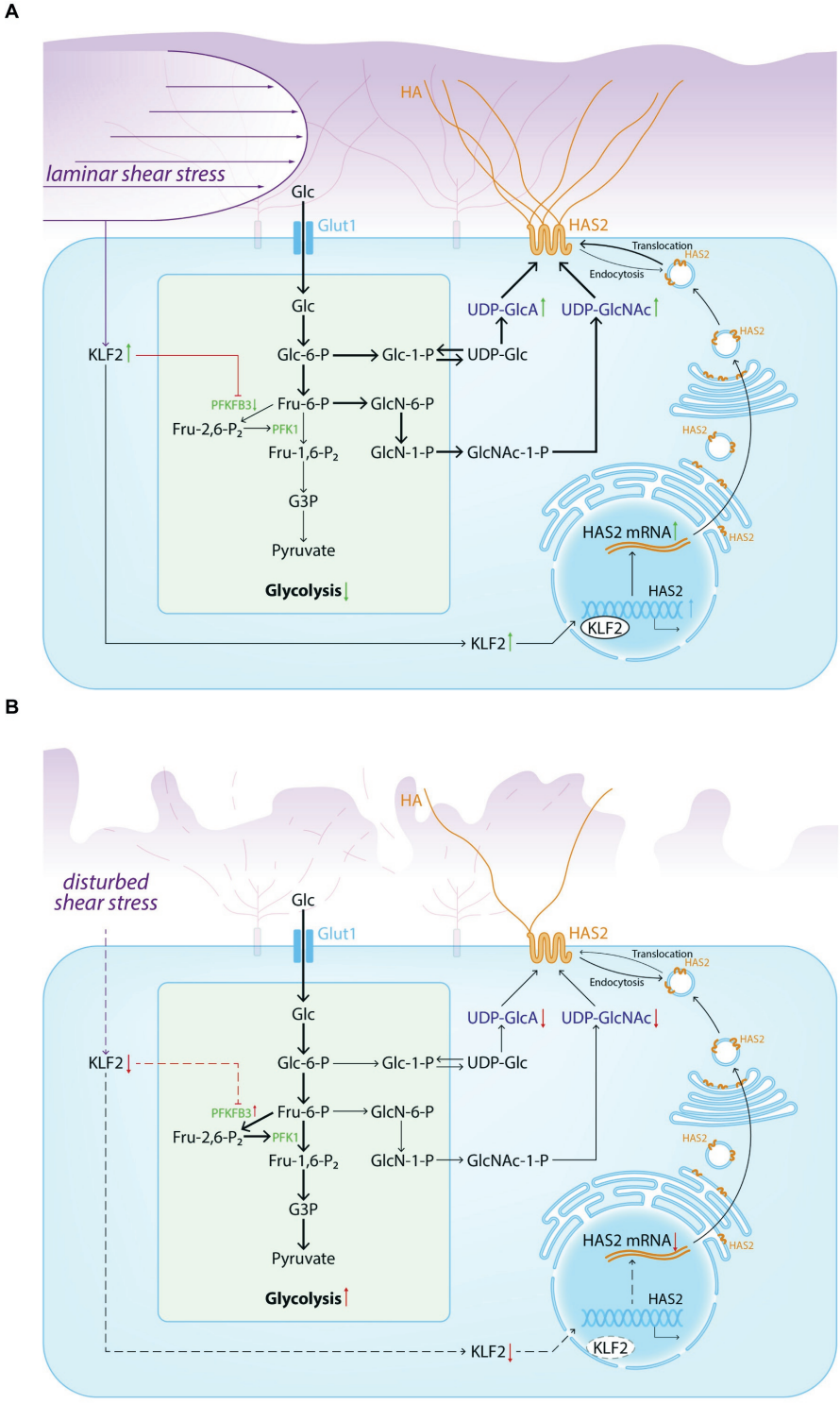
A
laminar shear stress
HA
Glc
Glut1
HAS2
Translocation
Endocytosis
HAS2
Glc
UDP-GlcA↑
UDP-GlcNAc↑
KLF2↑
Glc-6-P
Glc-1-P
UDP-Glc
PFKFB3↓
Fru-6-P
GlcN-6-P
Fru-2,6-P2
PFK1
Fru-1,6-P2
GlcN-1-P
GlcNAc-1-P
G3P
Pyruvate
Glycolysis↓
HAS2 mRNA↑
HAS2
KLF2
KLF2↑
B
disturbed
shear stress
HA
Glc
Glut1
HAS2
Translocation
Endocytosis
HAS2
Glc
UDP-GlcA↓
UDP-GlcNAc↓
KLF2↓
Glc-6-P
Glc-1-P
UDP-Glc
PFKFB3↑
Fru-6-P
GlcN-6-P
Fru-2,6-P2
PFK1
Fru-1,6-P2
GlcN-1-P
GlcNAc-1-P
G3P
Pyruvate
Glycolysis↑
HAS2 mRNA↓
HAS2
KLF2
KLF2↓

Figure 7. Schematic overview of the shear stress regulated endothelial hyaluronan production. (A) Laminar shear stress induces endothelial HA production through KLF2 activation and subsequent inhibition of the glycolytic activator PFKFB3, which allows glucose intermediates to shuttle into the biosynthetic pathways of UDP-GlcA and UDP GlcNAc and meanwhile increases surface HAS2 presence through regulating HAS2 mRNA transcription and protein translocation. (B) Disturbed shear stress reduces endothelial HA production by limiting both surface HAS2 enzyme and its substrates availability.

Part of the loss of endothelial glycocalyx in conditions such as diabetes and cancer may be explained by increased activity of glycocalyx degrading enzymes such as heparanase and hyaluronidase [42]. However, it must be assumed that glycocalyx thickness is the resultant of synthesis and degradation. While the synthesis of heparan sulfate and chondroitin sulfate occurs in the Golgi, HA is synthesized directly at the plasma membrane from its precursor molecules, rendering its synthesis dependent upon substrate availability, as indeed is shown in the current study. We recently demonstrated, using an inducible endothelial specific deletion of *has2* in mice, that loss of HA from the endothelial glycocalyx results in collapse of the glycocalyx, capillary destabilization and loss of endothelial barrier function[36]. It is therefore of interest therapeutically that cytosolic HA substrate availability can be increased by slowing down endothelial glycolysis as well as by increasing the extracellular concentrations of these substrates. Apart from the shear-KLF2 pathway, which has previously been shown to inhibit the key glycolysis regulator PFKFB3 [8], direct pharmacological inhibition of PFKFB3 has also been shown to be possible [43]. In the current study we confirm that the PFKFB3 inhibitor 3PO can restore loss of endothelial HA during oscillatory flow.

In mammalian cells, the three HAS isoenzymes (HAS1, HAS2, and HAS3) differ in distribution and enzyme properties and in response to different stimuli [5, 6, 44]. Among the three HASs, HAS1 expression is the lowest in healthy cells [45] and it requires higher concentration of substrates for HA synthesis [46], while HAS3 was shown to produce shortest molecular weight HA [5]. HAS2 is the most widespread isoform which is also correlated to HA distribution [6]. All three HASs have been shown to produce extracellular HA on the membrane, while HAS1 also produces intracellular HA [45]. We show that in endothelial cells HAS2 is the main enzyme to produce surface HA. HAS2 can be rapidly mobilized and transported to the plasma membrane for activation upon laminar shear [6, 23]. The exact mechanism of how shear also increases HAS2 protein concentrations still needs to be established, but could be related to the fact that HAS2 has been shown to be stabilized by *O*-GlcNAcylation [47].

CRISPR-Cas9 has been used to insert exogenous sequences into specific genomic sites via homology directed repair [48]. Cas9-mediated protein tagging simplified experimental analysis of protein function.

However, knock-in of fluorescent tags (i.e. GFP or RFP) to proteins can change its normal behaviour within the cell [49]. Here we inserted a small tetra cysteine tag (TC-tag, Cys-Cys-Pro-Gly-Cys-Cys) into the C-terminal end of the *HAS2* gene, using a non-viral Cas9 ribonucleoprotein system in primary endothelial cells [50]. Once the non-fluorescent FlAsH-EDT2 and ReAsH-EDT2 labelling reagents bind the TC-tag fused protein, the reagents will be converted to a highly fluorescent state [51]. We developed a genomic labelling technique of *HAS2* in primary endothelial cells that can be used to determine endogenous HAS2 expression and localization in live cells, and it also can be potentially applied to determine HAS2 protein stability and recycling capacity using time-lapse confocal microscopy.

In summary, we showed that quiescent endothelial cells, induced by prolonged laminar shear stress, presented a thicker glycocalyx HA on the surface through KLF2 regulated HAS2 expression and UDP-sugar availability. HAS2 was determined as the main hyaluronan synthase for HA in endothelial cells, regulated by UDP-GlcA. Endothelial cells need proper amount of HA to keep its integrity, which is likely determined by the metabolic state of endothelial cells, such as found under laminar shear stress.

Acknowledgments

We thank Cleveland Clinics to provide the online protocol for HA size analysis (NHLBI # PO1HL107147).

Sources of Funding

Financial Support by the Dutch Kidney Foundation (grants C08.2265) and the China Scholarship Council grant to Gangqi Wang (CSC no. 201406170050) are gratefully acknowledged.

Disclosure

None.

References

[1] Reitsma S, Slaaf DW, Vink H, van Zandvoort MA, oude Egbrink MG: The endothelial glycocalyx: composition, functions, and visualization. Pflugers Arch 2007, 454:345-59.
[2] Weinbaum S, Tarbell JM, Damiano ER: The structure and function of the endothelial glycocalyx layer. Annual review of biomedical engineering 2007, 9:121-67.
[3] Lewis JC, Taylor RG, Jones ND, St Clair RW, Cornhill JF: Endothelial surface characteristics in pigeon coronary artery atherosclerosis. I. Cellular alterations during the initial stages of dietary cholesterol challenge. Lab Invest 1982, 46:123-38.

[4] van den Berg BM, Spaan JA, Rolf TM, Vink H: Atherogenic region and diet diminish glycocalyx dimension and increase intima-to-media ratios at murine carotid artery bifurcation. American journal of physiology 2006, 290:H915-20.
[5] Itano N, Sawai T, Yoshida M, Lenas P, Yamada Y, Imagawa M, Shinomura T, Hamaguchi M, Yoshida Y, Ohnuki Y, Miyauchi S, Spicer AP, McDonald JA, Kimata K: Three isoforms of mammalian hyaluronan synthases have distinct enzymatic properties. The Journal of biological chemistry 1999, 274:25085-92.
[6] Torronen K, Nikunen K, Karna R, Tammi M, Tammi R, Rilla K: Tissue distribution and subcellular localization of hyaluronan synthase isoenzymes. Histochemistry and cell biology 2014, 141:17-31.
[7] Moretto P, Karousou E, Viola M, Caon I, D'Angelo ML, De Luca G, Passi A, Vigetti D: Regulation of Hyaluronan Synthesis in Vascular Diseases and Diabetes. Journal of diabetes research 2015, 2015:167283.
[8] Doddaballapur A, Michalik KM, Manavski Y, Lucas T, Houtkooper RH, You X, Chen W, Zeiher AM, Potente M, Dimmeler S, Boon RA: Laminar shear stress inhibits endothelial cell metabolism via KLF2-mediated repression of PFKFB3. Arteriosclerosis, thrombosis, and vascular biology 2015, 35:137-45.
[9] Meuwese MC, Broekhuizen LN, Kuikhoven M, Heeneman S, Lutgens E, Gijbels MJ, Nieuwdorp M, Peutz CJ, Stroes ES, Vink H, van den Berg BM: Endothelial surface layer degradation by chronic hyaluronidase infusion induces proteinuria in apolipoprotein E-deficient mice. PloS one 2010, 5:e14262.
[10] Huxley VH, Wang J, Whitt SP: Sexual dimorphism in the permeability response of coronary microvessels to adenosine. American journal of physiology 2005, 288:H2006-13.
[11] Jaffe EA, Nachman RL, Becker CG, Minick CR: Culture of human endothelial cells derived from umbilical veins. Identification by morphologic and immunologic criteria. The Journal of clinical investigation 1973, 52:2745-56.
[12] Hosoya T, Maruyama A, Kang MI, Kawatani Y, Shibata T, Uchida K, Warabi E, Noguchi N, Itoh K, Yamamoto M: Differential responses of the Nrf2-Keap1 system to laminar and oscillatory shear stresses in endothelial cells. The Journal of biological chemistry 2005, 280:27244-50.
[13] Chatzizisis YS, Coskun AU, Jonas M, Edelman ER, Feldman CL, Stone PH: Role of endothelial shear stress in the natural history of coronary atherosclerosis and vascular remodeling: molecular, cellular, and vascular behavior. J Am Coll Cardiol 2007, 49:2379-93.
[14] Zhang H, Baader SL, Sixt M, Kappler J, Rauch U: Neurocan-GFP fusion protein: a new approach to detect hyaluronan on tissue sections and living cells. J Histochem Cytochem 2004, 52:915-22.
[15] Boels MG, Avramut MC, Koudijs A, Dane MJ, Lee DH, van der Vlag J, Koster AJ, van Zonneveld AJ, van Faassen E, Grone HJ, van den Berg BM, Rabelink TJ: Atrasentan Reduces Albuminuria by Restoring the Glomerular Endothelial Glycocalyx Barrier in Diabetic Nephropathy. Diabetes 2016, 65:2429-39.
[16] van der Veer EP, de Bruin RG, Kraaijeveld AO: Quaking, an RNA-binding protein, is a critical regulator of vascular smooth muscle cell phenotype. Circulation research 2013, 113:1065-75.
[17] Simpson MA, Wilson CM, Furcht LT, Spicer AP, Oegema TR, Jr., McCarthy JB: Manipulation of hyaluronan synthase expression in prostate adenocarcinoma cells alters pericellular matrix retention and adhesion to bone marrow endothelial cells. The Journal of biological chemistry 2002, 277:10050-7.
[18] Wu H, Dmitriev I, Kashentseva E, Seki T, Wang M, Curiel DT: Construction and characterization of adenovirus serotype 5 packaged by serotype 3 hexon. Journal of virology 2002, 76:12775-82.
[19] Kostidis S, Addie RD, Morreau H, Mayboroda OA, Giera M: Quantitative NMR analysis of intra- and extracellular metabolism of mammalian cells: A tutorial. Analytica chimica acta 2017, in press.
[20] Vinaixa M, Rodriguez MA, Aivio S, Capellades J, Gomez J, Canyellas N, Stracker TH, Yanes O: Positional Enrichment by Proton Analysis (PEPA): A One-Dimensional (1) H-NMR Approach for (13) C Stable Isotope Tracer Studies in Metabolomics. Angewandte Chemie 2017, 56:3531-5.

[21] Dekker RJ, van Soest S, Fontijn RD, Salamanca S, de Groot PG, VanBavel E, Pannekoek H, Horrevoets AJ: Prolonged fluid shear stress induces a distinct set of endothelial cell genes, most specifically lung Kruppel-like factor (KLF2). Blood 2002, 100:1689-98.
[22] Cyphert JM, Trempus CS, Garantziotis S: Size Matters: Molecular Weight Specificity of Hyaluronan Effects in Cell Biology. International journal of cell biology 2015, 2015:563818.
[23] Hascall VC, Majors AK, De La Motte CA, Evanko SP, Wang A, Drazba JA, Strong SA, Wight TN: Intracellular hyaluronan: a new frontier for inflammation? Biochimica et biophysica acta 2004, 1673:3-12.
[24] Miller IJ, Bieker JJ: A Novel, Erythroid Cell-Specific Murine Transcription Factor That Binds to the Caccc Element and Is Related to the Kruppel Family of Nuclear Proteins. Molecular and cellular biology 1993, 13:2776-86.
[25] Zhang P, Basu P, Redmond LC, Morris PE, Rupon JW, Ginder GD, Lloyd JA: A functional screen for Kruppel-like factors that regulate the human gamma-globin gene through the CACCC promoter element. Blood Cell Mol Dis 2005, 35:227-35.
[26] Vigetti D, Viola M, Karousou E, De Luca G, Passi A: Metabolic control of hyaluronan synthases. Matrix biology : journal of the International Society for Matrix Biology 2014, 35:8-13.
[27] Vigetti D, Ori M, Viola M, Genasetti A, Karousou E, Rizzi M, Pallotti F, Nardi I, Hascall VC, De Luca G, Passi A: Molecular cloning and characterization of UDP-glucose dehydrogenase from the amphibian Xenopus laevis and its involvement in hyaluronan synthesis. The Journal of biological chemistry 2006, 281:8254-63.
[28] Baggenstoss BA, Harris EN, Washburn JL, Medina AP, Nguyen L, Weigel PH: Hyaluronan synthase control of synthesis rate and hyaluronan product size are independent functions differentially affected by mutations in a conserved tandem B-X7-B motif. Glycobiology 2016, 27:154-64.
[29] Viola M, Karousou E, D'Angelo ML, Caon I, De Luca G, Passi A, Vigetti D: Regulated Hyaluronan Synthesis by Vascular Cells. International journal of cell biology 2015, 2015:208303.
[30] Slawson C, Copeland RJ, Hart GW: O-GlcNAc signaling: a metabolic link between diabetes and cancer? Trends in biochemical sciences 2010, 35:547-55.
[31] Tarbell JM, Cancel LM: The glycocalyx and its significance in human medicine. Journal of internal medicine 2016.
[32] Broekhuizen LN, Mooij HL, Kastelein JJ, Stroes ES, Vink H, Nieuwdorp M: Endothelial glycocalyx as potential diagnostic and therapeutic target in cardiovascular disease. Current opinion in lipidology 2009, 20:57-62.
[33] Lee DH, Dane MJ, van den Berg BM, Boels MG, van Teeffelen JW, de Mutsert R, den Heijer M, Rosendaal FR, van der Vlag J, van Zonneveld AJ, Vink H, Rabelink TJ, group NEOs: Deeper penetration of erythrocytes into the endothelial glycocalyx is associated with impaired microvascular perfusion. PloS one 2014, 9:e96477.
[34] Yung S, Thomas GJ, Davies M: Induction of hyaluronan metabolism after mechanical injury of human peritoneal mesothelial cells in vitro. Kidney Int 2000, 58:1953-62.
[35] Dyer DP, Thomson JM, Hermant A, Jowitt TA, Handel TM, Proudfoot AE, Day AJ, Milner CM: TSG-6 inhibits neutrophil migration via direct interaction with the chemokine CXCL8. Journal of immunology 2014, 192:2177-85.
[36] van den Berg BM, Wang G, Boels MGS, Avramut MC, Jansen E, Sol W, Lebrin F, Jan van Zonneveld A, de Koning EJP, Vink H, Grone HJ, Carmeliet P, van der Vlag J, Rabelink TJ: Glomerular Function and Structural Integrity Depend on Hyaluronan Synthesis by Glomerular Endothelium. J Am Soc Nephrol 2019:DOI: 10.1681/ASN.2019020192.
[37] Shyy YJ, Hsieh HJ, Usami S, Chien S: Fluid shear stress induces a biphasic response of human monocyte chemotactic protein 1 gene expression in vascular endothelium. Proceedings of the National Academy of Sciences of the United States of America 1994, 91:4678-82.
[38] Tzima E, Del Pozo MA, Kiosses WB, Mohamed SA, Li S, Chien S, Schwartz MA: Activation of Rac1 by shear stress in endothelial cells mediates both cytoskeletal reorganization and effects on gene expression. Embo Journal 2002, 21:6791-800.

[39] Tzima E, Irani-Tehrani M, Kiosses WB, Dejana E, Schultz DA, Engelhardt B, Cao G, DeLisser H, Schwartz MA: A mechanosensory complex that mediates the endothelial cell response to fluid shear stress. Nature 2005, 437:426-31.
[40] Vigetti D, Genasetti A, Karousou E, Viola M, Moretto P, Clerici M, Deleonibus S, De Luca G, Hascall VC, Passi A: Proinflammatory cytokines induce hyaluronan synthesis and monocyte adhesion in human endothelial cells through hyaluronan synthase 2 (HAS2) and the nuclear factor-kappaB (NF-kappaB) pathway. The Journal of biological chemistry 2010, 285:24639-45.
[41] Maroski J, Vorderwulbecke BJ, Fiedorowicz K, Da Silva-Azevedo L, Siegel G, Marki A, Pries AR, Zakrzewicz A: Shear stress increases endothelial hyaluronan synthase 2 and hyaluronan synthesis especially in regard to an atheroprotective flow profile. Experimental physiology 2011, 96:977-86.
[42] Rabelink TJ, van den Berg BM, Garsen M, Wang G, Elkin M, van der Vlag J: Heparanase: roles in cell survival, extracellular matrix remodelling and the development of kidney disease. Nature reviews Nephrology 2017, 13:201-12.
[43] Cantelmo AR, Conradi LC, Brajic A, Goveia J, Kalucka J, Pircher A, Chaturvedi P, Hol J, Thienpont B, Teuwen LA, Schoors S, Boeckx B, Vriens J, Kuchnio A, Veys K, Cruys B, Finotto L, Treps L, Stav-Noraas TE, Bifari F, Stapor P, Decimo I, Kampen K, De Bock K, Haraldsen G, Schoonjans L, Rabelink T, Eelen G, Ghesquiere B, Rehman J, Lambrechts D, Malik AB, Dewerchin M, Carmeliet P: Inhibition of the Glycolytic Activator PFKFB3 in Endothelium Induces Tumor Vessel Normalization, Impairs Metastasis, and Improves Chemotherapy. Cancer cell 2016, 30:968-85.
[44] Jacobson A, Brinck J, Briskin MJ, Spicer AP, Heldin P: Expression of human hyaluronan synthases in response to external stimuli. The Biochemical journal 2000, 348 Pt 1:29-35.
[45] Siiskonen H, Oikari S, Pasonen-Seppanen S, Rilla K: Hyaluronan synthase 1: a mysterious enzyme with unexpected functions. Frontiers in immunology 2015, 6:43.
[46] Rilla K, Oikari S, Jokela TA, Hyttinen JM, Karna R, Tammi RH, Tammi MI: Hyaluronan synthase 1 (HAS1) requires higher cellular UDP-GlcNAc concentration than HAS2 and HAS3. The Journal of biological chemistry 2013, 288:5973-83.
[47] Vigetti D, Deleonibus S, Moretto P, Karousou E, Viola M, Bartolini B, Hascall VC, Tammi M, De Luca G, Passi A: Role of UDP-N-acetylglucosamine (GlcNAc) and O-GlcNAcylation of hyaluronan synthase 2 in the control of chondroitin sulfate and hyaluronan synthesis. The Journal of biological chemistry 2012, 287:35544-55.
[48] Ran FA, Hsu PD, Wright J, Agarwala V, Scott DA, Zhang F: Genome engineering using the CRISPR-Cas9 system. Nature protocols 2013, 8:2281-308.
[49] Crivat G, Taraska JW: Imaging proteins inside cells with fluorescent tags. Trends in biotechnology 2012, 30:8-16.
[50] Dewari PS, Southgate B, McCarten K, Monogarov G, O'Duibhir E, Quinn N, Tyrer A, Leitner MC, Plumb C, Kalantzaki M, Blin C, Finch R, Bressan RB, Morrison G, Jacobi AM, Behlke MA, von Kriegsheim A, Tomlinson S, Krijgsveld J, Pollard SM: An efficient and scalable pipeline for epitope tagging in mammalian stem cells using Cas9 ribonucleoprotein. eLife 2018, 7.
[51] Hoffmann C, Gaietta G, Zurn A, Adams SR, Terrillon S, Ellisman MH, Tsien RY, Lohse MJ: Fluorescent labeling of tetracysteine-tagged proteins in intact cells. Nature protocols 2010, 5:1666-77.

Supplemental figures

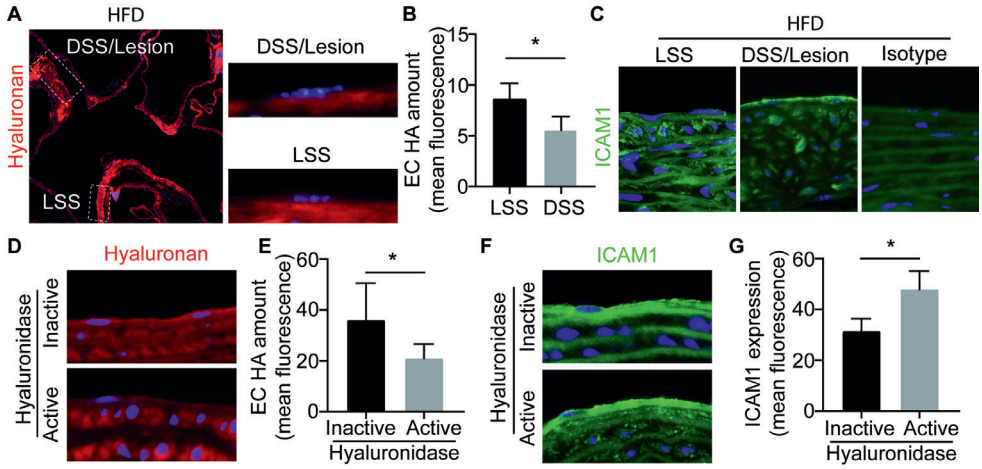

Figure I. **Loss of hyaluronan leads to endothelial activation in mouse aorta under high fat diet.** (A) Representative images of HA stained at the surface of the aortic region of *apoE*-KO mice on high fat diet (HFD, n=6). Area exposed to LSS or lesion area exposed to DSS are labelled with Ncan-dsRed. (B) Quantification of HA staining in LSS and DSS exposed aortic regions. (C) Representative images of ICAM1 stained at the aortic regions exposed to LSS and lesion region exposed to DSS. Rabbit IgG was used as an isotype control of ICAM1 staining. (D) Representative images of HA stained at the surface of the aortic region of *apoE*-KO mice on HFD treated with inactive (n=7) or active hyaluronidase (n=6) respectively. Areas exposed to LSS were presented. (E) Quantification of HA staining in LSS exposed aortic regions upon hyaluronidases treatments. (F) Representative images of ICAM1 stained at the aortic regions exposed to LSS upon hyaluronidases treatments on HFD. (G) Quantification of ICAM1 staining in LSS exposed aortic regions upon hyaluronidases treatments. Non-paired 2-tailed Student's t test was performed; *P < 0.05, **P < 0.01.

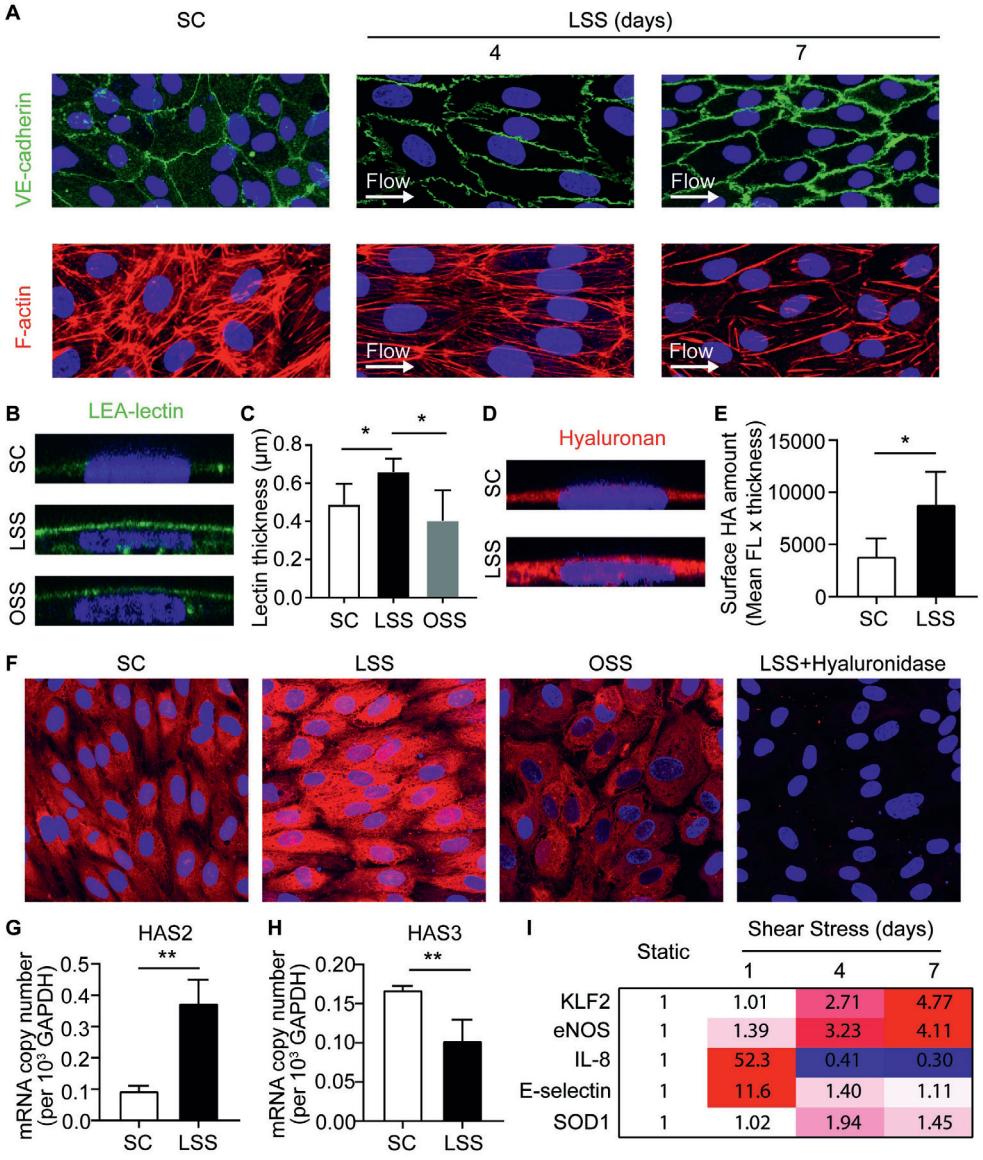

Figure II. **Prolonged shear stress induces quiescent endothelium and hyaluronan production.** (A) Cell morphology changes upon prolonged shear stress exposure. HUVECs stained with antibodies against VE-cadherin (top row) and the F-actin binding phalloidin-rhodamine (bottom row) to visualize endothelial phenotypic changes. Static cultured HUVECs (left) were compared to HUVECs cultured for 4 days (middle) and 7 days (right) exposed to 10dyne/cm^2 laminar shear stress. (B) Representative confocal images of lectin from *Lycopersicon esculentum* (LEA) staining in HUVECs after 4 days of static culture or exposure to shear stress. (C) Quantification of luminal LEA thickness in static culture or exposure to shear stress. (D) Representative confocal images of HA staining of HUVECs in SC or after

4 days LSS respectively. (E) Quantification of endothelial surface HA in different culture conditions. (F) Representative confocal images of HA staining of HUVECs in SC or after 4 days LSS, or after 4 days exposure to oscillatory shear stress (OSS) respectively. Hyaluronidase treatment was presented as a negative control of HA staining. (G) HAS2- and (H) HAS3 mRNA expression in SC or in response to LSS. (I) Heatmap of the relative selected genes expression for endothelial function that show reponse to shear stress of 1, 4 or 7 days (fold change compared to static culture). All values are given as mean ± SD of 4-5 independent experiments. Non-paired 2-tailed Student's t test and one-way ANOVA followed by Tukey test were performed; *P < 0.05, **P < 0.01.

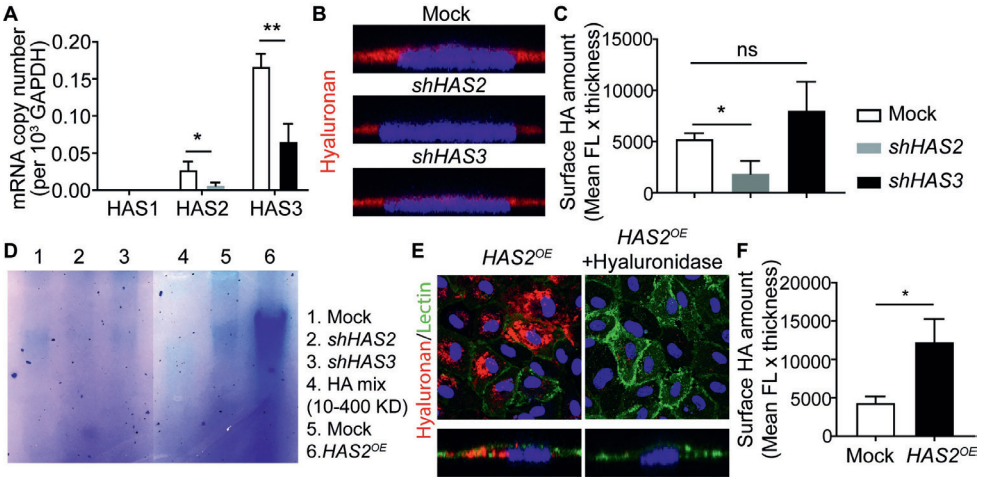

Figure III. **HAS2 is the main synthase responsible for HA synthesis in endothelial cells.** (A) HAS1, HAS2 and HAS3 mRNA expression in static cultured HUVECs, and changes after HAS2 (*shHAS2*) or HAS3 (*shHAS3*) knock-down, normalized to 10^3 copies *GAPDH*. (B) Representative confocal images of HA staining in HUVECs 3 days after transduction with *shHAS2* or *shHAS3*, and (C) surface HA quantification. (D) Representative agarose gel of HA size analysis after *shHAS2*, *shHAS3* or HAS2 overexpression (*HAS2^{OE}*) reveals that the majority of HA size is over 400KD. (E) Representative confocal images of HA staining in HUVECs after *HAS2^{OE}*, showing typical intracellular HA cable structures. Hyaluronidase treatment was presented as a negative control of HA staining. (F) Quantification of surface HA amount after *HAS2^{OE}*. All values are given as mean ± SD of 3 independent experiments. Non-paired 2-tailed Student's t test and one-way ANOVA followed by Tukey test were performed; *P < 0.05, **P < 0.01.

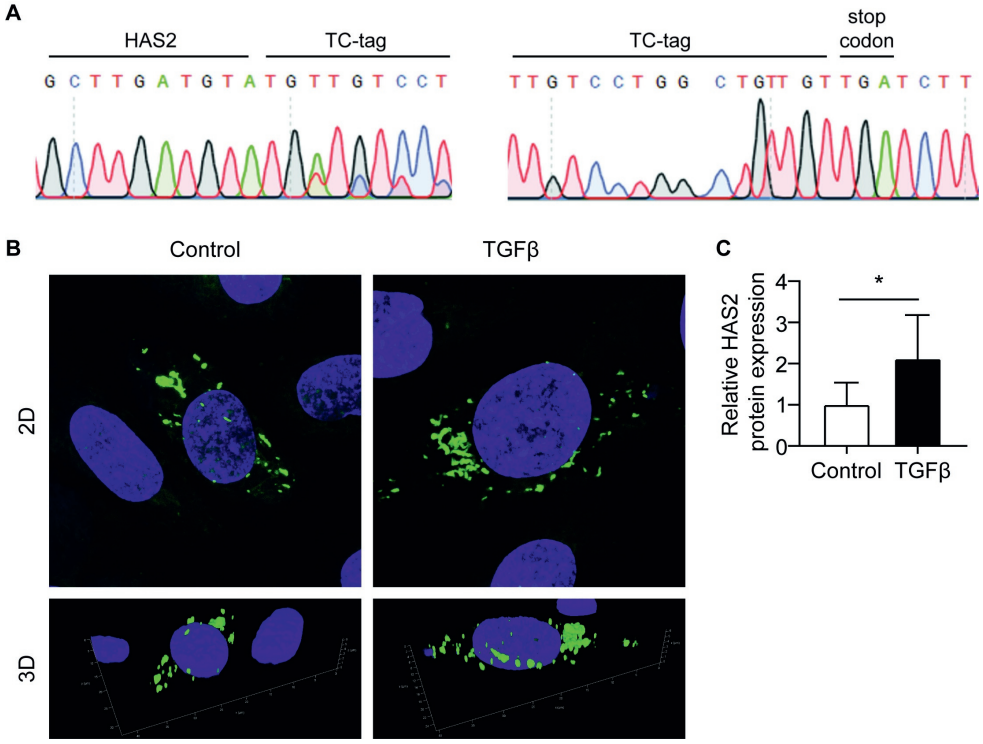

Figure IV. **Endogenous tagging of HAS2 using CAS9 ribonucleoprotein.** (A) The tetra cysteine tag (TC-tag) sequence "TGTTGTCCTGGCTGTTGT" was confirmed to be inserted in the end of HAS2 genome by DNA sequencing. (B) Representative images of HAS2-TC-tag protein expression with TGFβ in static culture. HAS2-TC tag visualized in 2D (top row) and 3D (bottom row). (C) Quantification of HAS2-TC-tag protein expression, presented as relative to static culture. A total of 12 cells from each group were imaged and quantified. Non-paired 2-tailed Student's t test was performed; *$P < 0.05$.

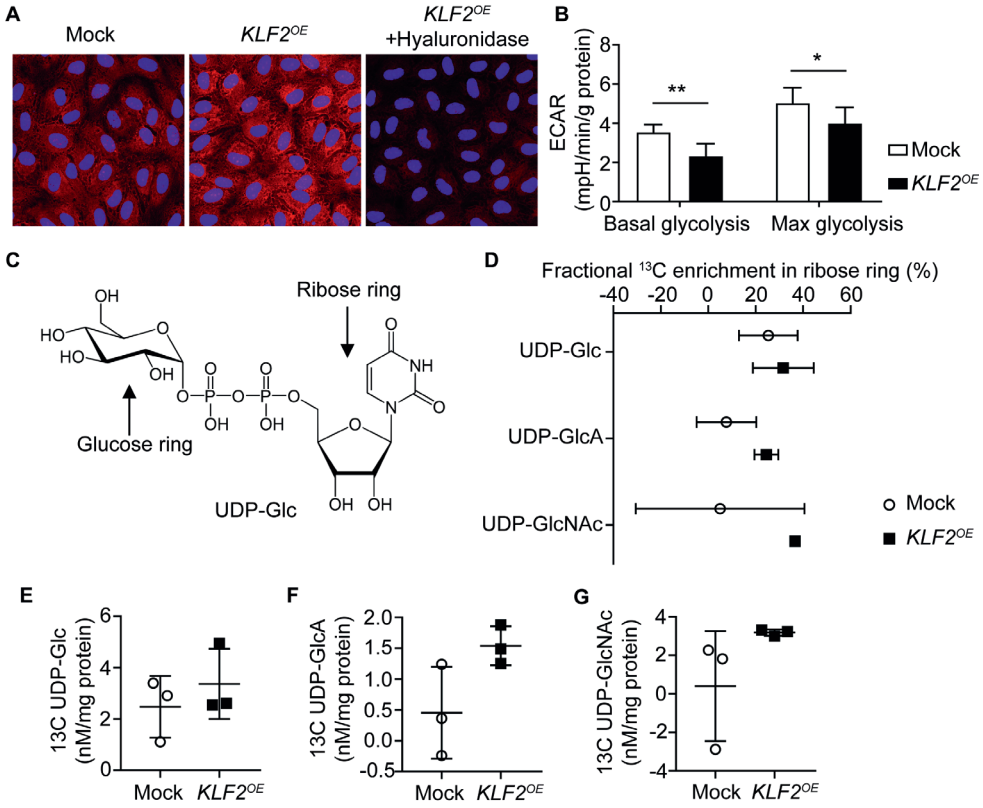

Figure V. **Concentration of intracellular UDP-sugar concentrations during high *KLF2* expression**. (A) Representative confocal images of HA staining of HUVECs upon *KLF2*^{OE}. Hyaluronidase treatment was presented as a negative control of HA staining. (B) Seahorse XF flux analysis of overall glycolytic capacity, quantified 48hrs after transduction of *KLF2*^{OE}. (C) Chemical structure representation of the glucose- and ribose ring of UDP-glucose. (D) Enrichment analysis of ^{13}C over ^{12}C labeling of the UDP-sugar ribose rings. To track the glucose flux to the UDP-sugar biosynthesis pathways, ^{13}C-labeled ribose rings of (E) UDP-Glc, (F) UDP-GlcA and (G) UDP-GlcNAc were quantified. All values are given as mean ± SD of 3 independent experiments. Non-paired 2-tailed Student's t test was performed; *P < 0.05, **P < 0.01.

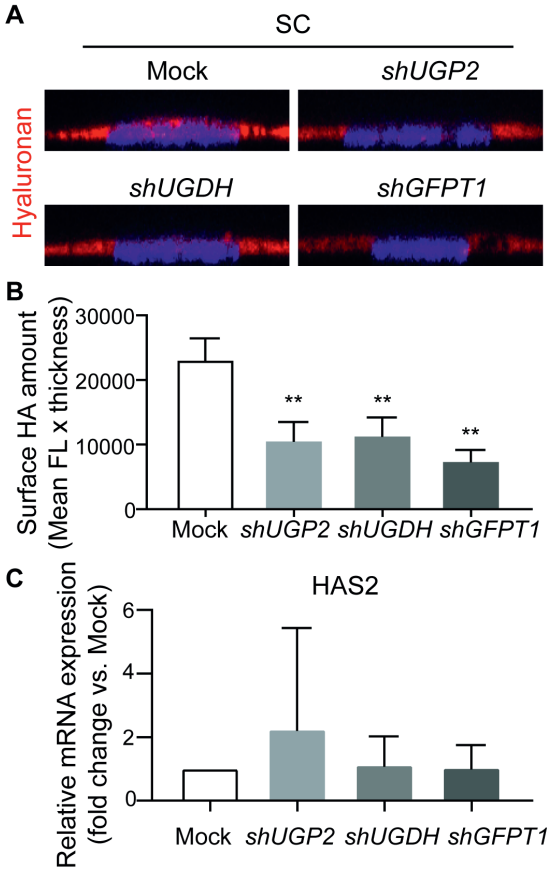

Figure VI. **Role of key rate-limiting enzymes in HA substrate production in static endothelial cell culture.** (A) Representative confocal images of HA staining in HUVECs after knockdown of the key rate-limiting enzymes UDP-glucose pyrophosphorylase 2 (*shUGP2*), UDP-glucose dehydrogenase (*shUGDH*), or glutamine-fructose-6-phosphate transaminase 1 (*shGFPT1*), after 4 days of static culture, and (B) quantification of surface HA. (C) HAS2 mRNA expression in HUVECs after knockdown of UGP2, UGDH or GFPT1. All values are given as mean ± SD of 3 independent experiments. Non-paired 2-tailed Student's t test and one-way ANOVA followed by Tukey test were performed; *P < 0.05, **P < 0.01.

Supplemental Tables

Table I Primers used for RT-PCR or genotyping

	Forward (5'-3')	*Reverse (5'-3')*	*Product (bp)*
HAS1	TCAAGGCGCTCGGAGATTC	CTACCCAGTATCGCAGGCT	*195*
HAS2	AAGAACAACTTCCACGAAAAGGG	GGCTGGGTCAAGCATAGTGT	*216*
HAS3	CAGCCTATGTGACGGGCTAC	CCTCCTGGTATGCGGCAAT	*210*
KLF2	CTACACCAAGAGTTCGCATCTG	CCGTGTGCTTTCGGTAGTG	*137*
PFKFB3	CAGTTGTGGCCTCCAATATC	GGCTTCATAGCAACTGATCC	*113*
NOS3	TGATGGCGAAGCGAGTGAAG	ACTCATCCATACACAGGACCC	*129*
ICAM1	GTATGAACTGAGCAATGTGCAAG	GTTCCACCCGTTCTGGAGTC	*119*
IL-8	ACTGAGAGTGATTGAGAGTGGAC	AACCCTCTGCACCCAGTTTTC	*112*
E-selectin	CAGCAAAGGTACACACACCTG	CAGACCCACACATTGTTGACTT	*128*
SOD1	GGTGGGCCAAAGGATGAAGAG	CCACAAGCCAAACGACTTCC	*227*
HAS2-wt	AATAAGTGTGGCAGGCGGAA	TCAGGCGGATGCACAGTAAG	*323*
HAS2-mut	TGTCCTGGCTGTTGTTGATCT	AAACACTTTCAGGCGGATGC	*292*